Dyes and Pigments 89 (2011) 37–43

Contents lists available at ScienceDirect

Dyes and Pigments

journal homepage: www.elsevier.com/locate/dyepig

# Crystal structure prediction of organic materials: Tests on the 1,4-diketo-3,6-diphenylpyrrolo(3,4-c)pyrrole and 1,4-diketo-3,6-bis(4′-dipyridyl)-pyrrolo-[3,4-c]pyrrole

Kyung-Hyun Kim [a], Dong Hyun Jung [a], Daejin Kim [a], Areum Lee [a], Kihang Choi [b], Yongho Kim [c], Seung-Hoon Choi [a,*]

[a] Insilicotech Co. Ltd., A-1101, Kolontripolis, 210, Geumgok-Dong, Bundang-Gu, Seongnam-Shi 463-943, Republic of Korea
[b] Department of Chemistry, Korea University, 1, Anam-dong 5-Ga, Seongbuk-Gu, Seoul 136-701, Republic of Korea
[c] Department of Chemistry, Kyung Hee University, 1 Seochun-Dong, Kiheung-Gu, Yongin-City, Gyunggi-Do 449-701, Republic of Korea

ARTICLE INFO

*Article history:*
Received 22 June 2010
Accepted 27 August 2010
Available online 19 September 2010

*Keywords:*
Crystal structure prediction
Pigments
DPP
DPPP
Monte Carlo simulation
Polymorphism

ABSTRACT

The crystal structures of a yellowish-red pigment, 1,4-diketo-3,6-diphenylpyrrolo(3,4-c)pyrrole (DPP), and its derivative with high proton affinity, 1,4-diketo-3,6-bis(4′-dipyridyl)-pyrrolo-[3,4-c]pyrrole(DPPP), were predicted using Polymorph Predictor in Materials Studio 4.4. The possible structures were generated using Monte Carlo method and they were minimized with COMPASS and Dreiding forcefields. Among the predicted structures with the space groups same as those of the experimental X-ray crystal structures, structures fitting best to the experimental structures were searched. The resulting structures are in good agreement with the experimental structures showing that Monte Carlo simulated annealing is an efficient method for predicting crystal structures of DPP derivatives.



## 1. Introduction

Organic and inorganic pigments are essential materials for paint, ink, cosmetic and synthetic fiber industries. Pigments are also key components for display devices such as LCD and OLED, and the recent increased demand for innovative display devices has caused extensive studies on organic pigments [1,2]. In general, pigment molecules can be tightly stacked by π–π interaction and retain the crystalline features during the whole chemical engineering processes. Thus, the main physicochemical properties of pigments, such as color, brightness, light fastness and saturation, are greatly affected by the crystal packing and morphology. Determination of crystal structure and morphology is very difficult and time consuming [3], and therefore crystal structures of many useful pigments are still unknown. If the crystal structures can be predicted precisely by computational methods, the physical and chemical properties of pigments would be better understood and therefore be more easily controlled. Crystal structure prediction (CSP) could also find applications in research areas such as pharmaceutics, hydrogen storage, functional fibers and other related with crystalline materials.

During the last decade, many research groups tried CSP for small organic molecules using various computational approaches [4–9]. Four times of CSP blind tests have been held by the Cambridge Crystallographic Data Center (CCDC) [10–13] and many research groups took part in the tests. In spite of the continued efforts, there are many remaining problems to be solved, such as the limitation on the number of total atoms and asymmetric units.

In this study, we have predicted the crystal structures of two organic pigments with different packing structures and then compared the structures and the simulated X-ray powder diffraction (XRPD) patterns with the experimental data. The first pigment studied is 1,4-diketo-3,6-diphenylpyrrolo(3,4-c)pyrrole(DPP) [14], or C.I. Pigment Red 255, which is yellowish red, and used in conventional paint and ink applications, refinish, PVC, EL, and color filters for LCD. The second pigment is 1,4-diketo-3,6-bis(4′-dipyridyl)-pyrrolo-[3,4-c]-pyrrole (DPPP) [15], a dipyridyl derivative of DPP. Particularly, DPPP has two crystal phases with different space

* Corresponding author. Tel.: +82 31 728 0443; fax: +82 31 728 0444.
*E-mail address:* shchoi@insilicotech.co.kr (S.-H. Choi).

0143-7208/$ – see front matter © 2010 Elsevier Ltd. All rights reserved.
doi:10.1016/j.dyepig.2010.08.017

groups and, because of the high proton affinity of the pyridine N atom, it can be used for $H_2$ sensing or storage [15]. The chemical structures of DPP and DPPP molecules are shown in Fig. 1 and the crystallographic information is listed in Table 1. Both the molecules have two rotatable bonds between the core structure and aromatic rings. Interestingly, the torsional angles of these rotatable bonds are different for DPP and DPPP affecting their crystal packing structures. We tried CSP with and without considering the conformational degrees of freedom and compared the results, particularly for DPPP.

## 2. Computational details and crystal structure prediction

We optimized molecular structures at the level of Hartree–Fock with 6-31G(d) basis set and calculated electrostatic potential derived (ESPD) point charges based on the optimized structures using GAUSSIAN03 [16]. The optimized structure was then used as the main input for the following polymorph packing runs. The polymorphic prediction was performed using the Polymorph Predictor module in Materials Studio 4.4 (MS 4.4) [17]. In this process, the input molecule was constrained as a rigid entity so that the intramolecular forces are fixed and only the intermolecular interactions become important in determining the lattice energy of predicted structures.

Thousands of crystal packing structures with a desired space group were generated by the Monte Carlo simulated annealing method. The subgroup of the desired space group was also searched because the intramolecular symmetry may not be properly treated during the CSP process. These structures were clustered based on their structural similarity and cell formula, and then subjected to the energy minimization using the selected forcefield with Ewald summation. Finally, the predicted structures were clustered again, and then ranked according to the lattice energy. These structures are indexed as (*n*th run)-(space group)-(ranking of energy); for example, structure 4-P$\bar{1}$-1 is the one ranked at the first place in the 4th run for P$\bar{1}$ space group. We tested COMPASS [18–20] and Dreiding 2.21 [21] as the forcefield, and used the ESPD point charges for electrostatic energy calculation.

In order to compare the predicted structures to the experimental X-ray crystal structures, the powder diffraction patterns were simulated with the Reflex Plus module in Materials Studio 4.4. The XRPD patterns simulated for the X-ray and predicted structures were obtained with 2Θ angles ranging from 2° to 35°, using Cu *Kα* radiation with wavelength of 1.5406 Å. All the X-ray crystal structures were obtained from CCDC.

**Table 1**
The Crystallographic information of 1,4-diketo-3,6-diphenylpyrrolo(3,4-c)pyrrole (DPP) and 1,4-diketo-3,6-bis(4′-dipyridyl)-pyrrolo-[3,4-c]pyrrole(DPPP).

| | DPP | DPPP | |
|---|---|---|---|
| | | Phase I | Phase II |
| Space Group | P$\bar{1}$ | $P2_1/n$ | $P2_1/c$ |
| Z | 1 | 2 | 4 |
| a | 3.817 | 3.722 | 3.695 |
| b | 6.516 | 6.263 | 18.201 |
| c | 13.531 | 26.506 | 18.456 |
| α | 93.11 | 90.00 | 90 |
| β | 86.97 | 94.41 | 94.680 |
| γ | 95.02 | 90.00 | 90 |
| Cell $V/Z$[Å$^3$] | 334.4 | 616.0 | 1237.1 |
| $\rho$[g/cm$^3$] | 1.425 | 1.565 | 1.559 |

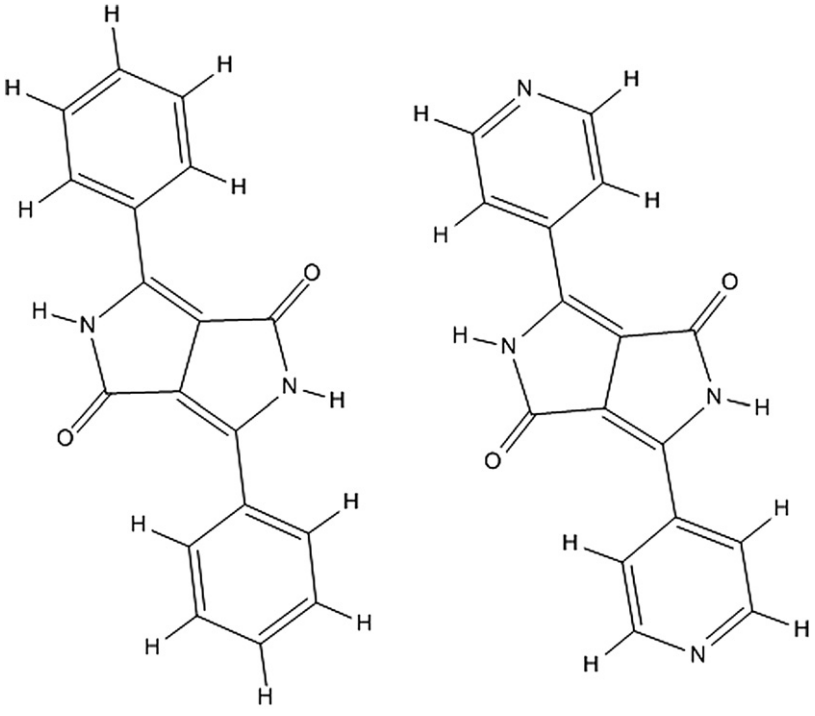


**Fig. 1.** Chemical structures of (a) 1,4-diketo-3,6-diphenylpyrrolo(3,4-c)pyrrole(DPP) and (b) 1,4-diketo-3,6-bis(4′-dipyridyl)-pyrrolo-[3,4-c]pyrrole(DPPP).

## 3. Results and discussion

### 3.1. DPP

DPP is a yellowish-red pigment with excellent hiding power and outdoor durability, and has many industrial applications. Only one polymorph of DPP has been reported so far (CCDC reference code SAPDES) and its packing shapes and structures are shown in Fig. 2. All the molecules in the crystal lie parallel to one another and the packing shapes are very similar to those of α-quinacridone and α-copper phthalocyanine. The crystal structure of DPP has triclinic (space group Pī) symmetry and its crystallographic parameters are listed in Table 1.

As previous studies [4,5,7] had suggested, we calculated the atomic ESPD charges using Hartree–Fock method with 6-31G(d) basis set. When we used other point charges calculated by QEq [22] or Gasteiger [23] methods, no simulated structure was found similar to the X-ray crystal structure.

After four consecutive packing runs with Dreiding or COMPASS forcefield, about 3900 crystal structures were generated for each forcefield. The structures obtained using Dreiding forcefield showed lattice energies ranging from −8.6 to 60.6 kcal/mol, and the ones fitting well to the X-ray structure were found in the low energy and high density region as shown in Fig. 3a. The two best fitting structures, 4-Pī-1 and 4-P1-1, are the ones ranked first for the lowest lattice energy among the structures obtained in the fourth run for Pī and P1 space groups, respectively. The crystallographic information on these best structures is listed in Table 2. We also performed predicting calculations four times consecutively using COMPASS forcefield and obtained about 15,249 predicted structures. The lattice energy was ranging from −161.69 to −115.01 kcal/mol and the energy–density plot is shown at Fig. 3b. We could find the best matched structures at the first place energy ranking for P1 space group in the first run in the total prediction calculations. The XRPD patterns simulated on the basis of the X-ray and the predicted crystal structures of DPP are in good agreement with each other (Fig. 4). Fig. 5 shows that structure 1-P1-1 predicted with COMPASS forcefield superimposes well with the X-ray structure.

### 3.2. DPPP

DPPP is a dipyridyl derivative of DPP with high proton affinity. Protonation at the pyridine N atoms induces color change from vivid red to violet and, because of this property, DPPP can be utilized for $H_2$ gas sensing. Mizuguchi et al. reported two different crystal structures, phase I and II, of DPPP [24] and their crystallographic data and packing shapes are summarized in Table 1 and Figs. 6 and 7, respectively. The molecular conformations are different in the two phases and the molecule in phase II has different torsion angles of the two pyridine-linkage bonds. In the CSP, however, the input structure of DPPP optimized at the Hartree–Fock level has same torsion angles of the pyridine-linkage bonds, and this conformation is kept rigidly in the whole prediction process.

The lattice energy of 2373 structures predicted using COMPASS forcefield ranges from −124.8 to −79.1 kcal/mol. Among these, the structure best fitting to phase I is the one ranked first in the second run for $P2_1$ subgroup and the structure best fitting to phase II is the one ranked at the 32nd place in the first run for $P2_1/c$ space group. The crystallographic data of these simulated structures are listed in Table 3. Using Dreiding forcefield, we generated 3748 structures with lattice energies ranging from −17.9 to 19.3 kcal/mol. The best structure for phase I is at the third rank of energy in the fourth run

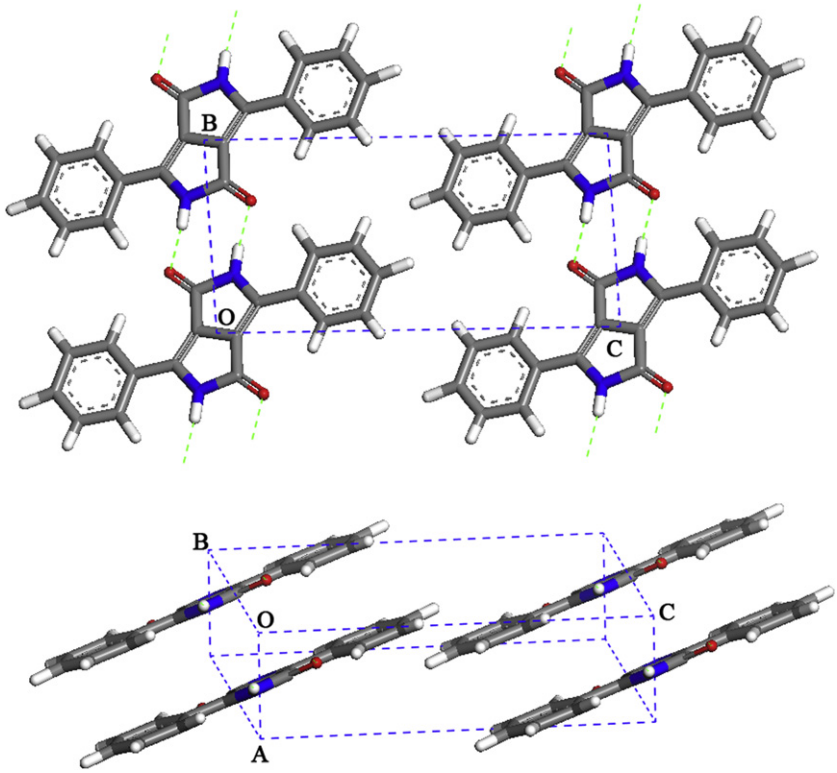


**Fig. 2.** The X-ray crystal structure of DPP.

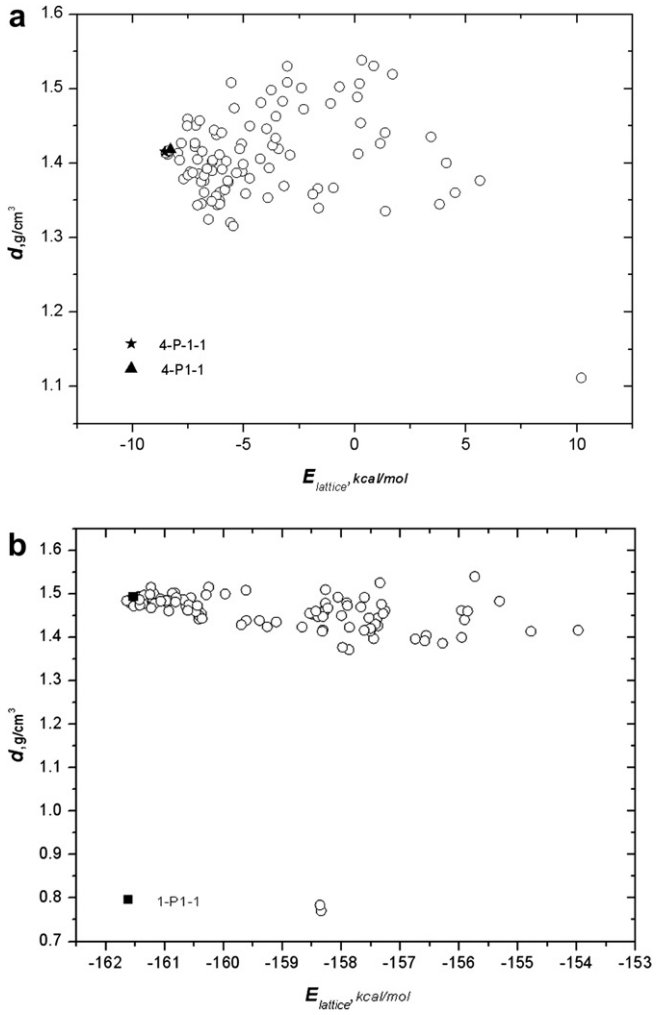


**Fig. 3.** Scatter plots of energy–density in the results of DPP structures predicted using (a) Dreiding forcefield and (b) COMPASS forcefield. Each solid symbol depicts the best fitted structure to the X-ray crystal structure.

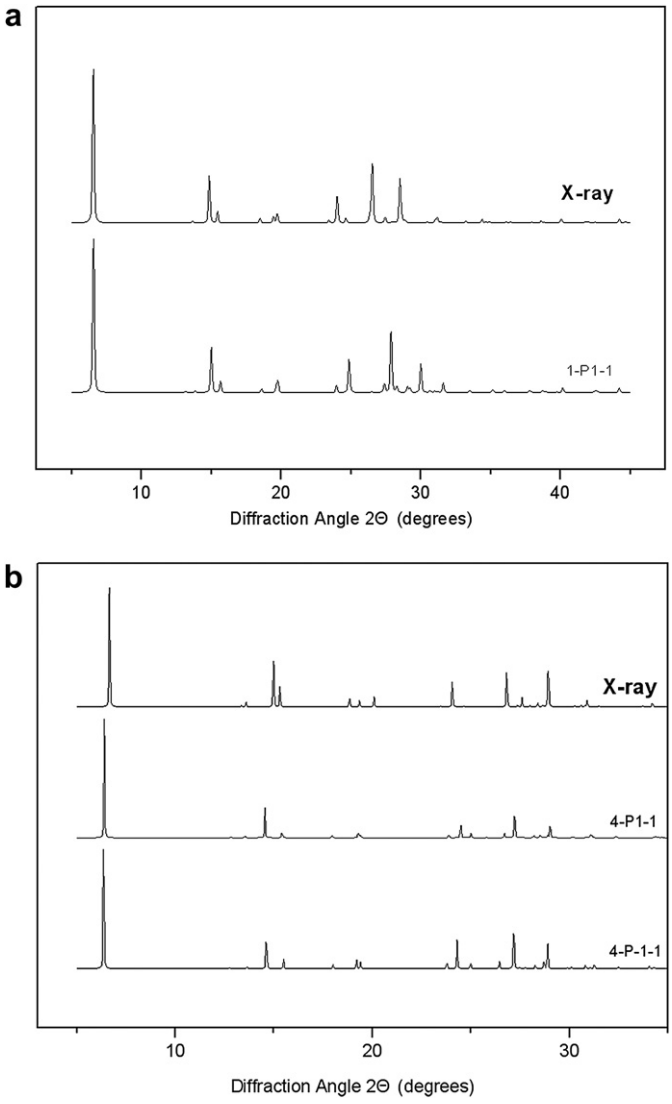


**Fig. 4.** The simulated powder patterns of the X-ray and predicted structures of DPP which are from the results with (a) Dreiding and (b) COMPASS forcefield.

for $P2_1$ space group and the best structure for phase II is at the 62nd rank in the first run for $P2_1/c$ group. In the energy–density plot (Fig. 8), the structures predicted for phase I are found in the low energy and high density region and the structures for phase II are found in the relatively high energy region.

**Table 2**
Crystallographic data and lattice energy for the predicted polymorph structures of DPP as obtained from the Polymorph Predictor with COMPASS and Dreiding forcefield in the energy calculations.

| Forcefield DPP | X-ray | COMPASS | Dreiding | |
|---|---|---|---|---|
| | | 1-P1-1 | 4-P$\bar{1}$-1 | 4-P1-1 |
| Space Group | P$\bar{1}$ | P1 | P$\bar{1}$ | P1 |
| a | 3.817 | 3.714 | 3.749 | 3.733 |
| b | 6.516 | 13.482 | 6.515 | 6.563 |
| c | 13.531 | 6.408 | 13.929 | 13.855 |
| α | 93.11 | 93.14 | 85.57 | 94.44 |
| β | 86.97 | 92.37 | 86.69 | 92.59 |
| γ | 95.02 | 89.69 | 87.16 | 86.91 |
| Cell $V$/Z[Å$^3$] | 334.4 | 320.1 | 338.3 | 337.623 |
| $\rho$[g/cm3] | 1.425 | 1.496 | 1.415 | 1.418 |
| $LE$[a](kcal/mol) | | −161.54 | −8.56 | −8.31 |

[a] Lattice Energy.

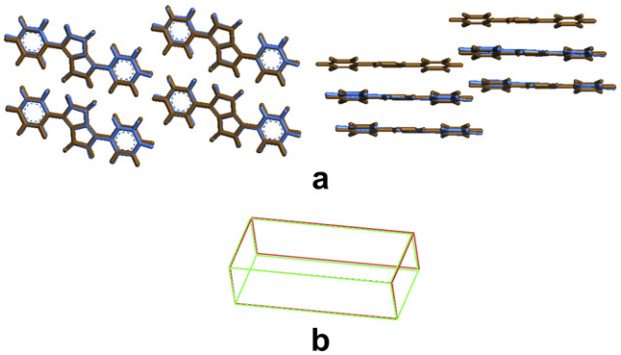


**Fig. 5.** (a) Comparison of the packing shapes of the X-ray structure (blue) and the simulated structure (brown) of DPP which was predicted with COMPASS forcefield. (b) An overlay of the unit cells of the X-ray (red) and predicted (green) structures. (For the interpretation of the reference to color in this figure legend the reader is referred to the web version of this article).

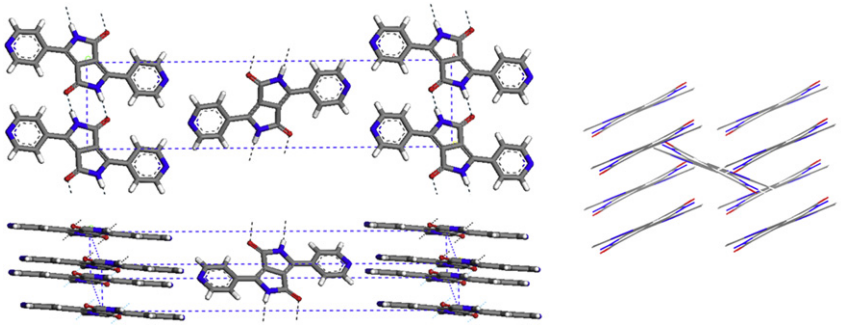

**Fig. 6.** X-ray crystal structure of DPPP in phase I. The dashed lines depict the hydrogen bonding in the crystal structure.

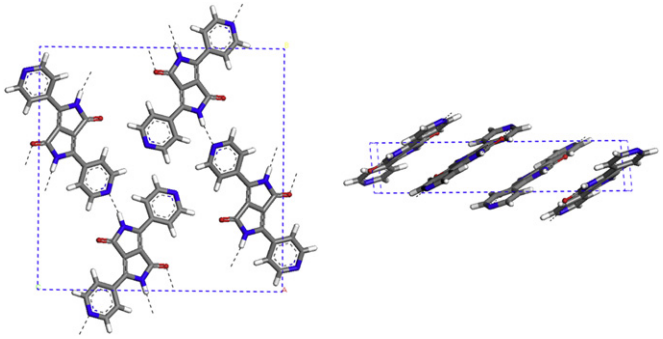

**Fig. 7.** X-ray crystal structure of DPPP in phase II. The dashed lines depict the hydrogen bonding in the crystal structure.

As shown in Fig. 9a, the simulated XRPD patterns of phase I are very similar for the X-ray structure and for the structure predicted using COMPASS forcefield. The predicted structure of DPPP in phase I is very well overlaid with the X-ray structure (Fig. 10). In the case of phase II, however, the XRPD patterns show small differences between the X-ray and the predicted structures (Fig. 9b). This is presumably because of the difference in the torsion angles: as mentioned above, the DPPP molecule in phase II has two different torsion angles of the pyridine-linkage bonds but the input molecule used in the prediction process has the same torsional angles for these rotatable bonds. Nevertheless, the packing shapes of the predicted phase II structure shown in Fig. 11 indicate that in spite of the different conformational structure of input molecule from the X-ray structure CSP process used in this work may generate reliable crystal structures. In fact, we also tried CSP using the input molecule with full conformational degrees of freedom, but we could not obtain structures similar to the phase II crystal structure. It seems that more simulation steps are required in the Monte Carlo calculation for the molecule with higher degree of freedom.

**Table 3**
Crystallographic data and lattice energy for the predicted two different polymorph structures of DPPP as obtained from the Polymorph Predictor with COMPASS and Dreiding forcefield in the energy calculations.

| | Phase I | | | Phase II | | |
|---|---|---|---|---|---|---|
| Forcefield | | Dreiding | COMPASS | | Dreiding | COMPASS |
| Structure | X-ray | 4-P21-3 | 2-P21-1 | X-ray | 1-$P2_1/c$-62 | 1-$P2_1/c$-32 |
| Space Group | $P2_1/n$ | $P2_1$ | $P2_1$ | $P2_1/n$ | $P2_1/c$ | $P2_1/c$ |
| a | 3.722 | 3.742 | 3.742 | 3.695 | 3.708 | 3.765 |
| b | 6.263 | 6.341 | 6.299 | 18.201 | 18.612 | 17.907 |
| c | 25.506 | 27.369 | 26.371 | 18.456 | 19.231 | 18.216 |
| α | 90.00 | 90.00 | 90.00 | 90.00 | 90.00 | 90.00 |
| β | 94.41 | 99.36 | 96.66 | 94.68 | 83.61 | 92.39 |
| γ | 90.00 | 90.00 | 90.00 | 90.00 | 90.00 | 90.00 |
| Cell $V$/Z[Å$^3$] | 616.0 | 640.77 | 612.70 | 1237.1 | 1318.8 | 1226.9 |
| $\rho$[g/cm3] | 1.565 | 1.505 | 1.573 | 1.559 | 1.462 | 1.571 |
| $LE$[a](kcal/mol) | | −17.32 | −124.76 | | −12.26 | −122.19 |

[a] Lattice Energy.

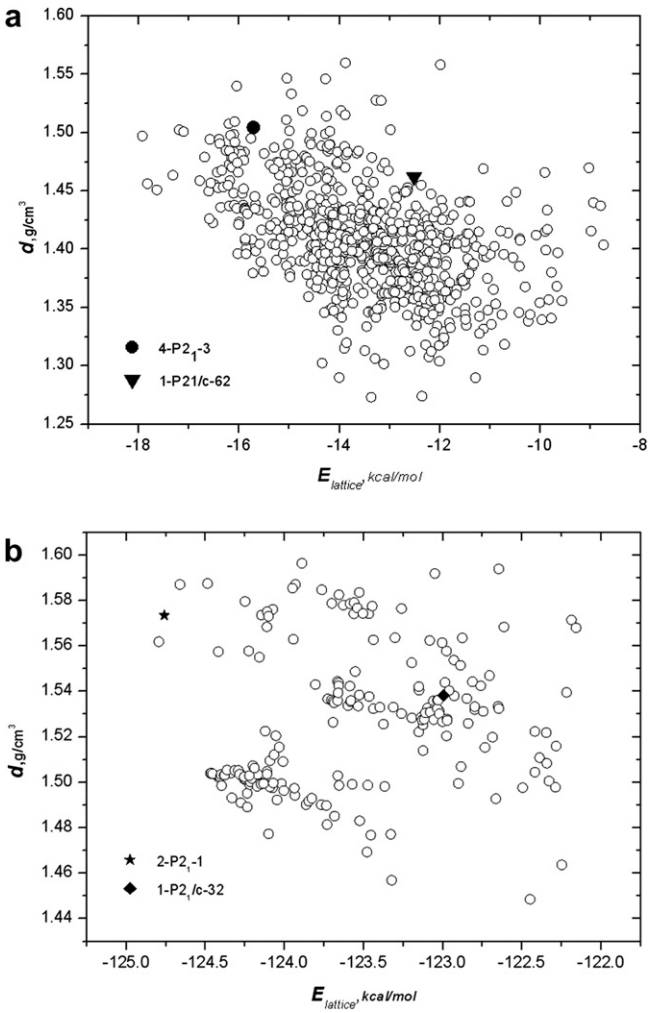


**Fig. 8.** Scatter plots of energy–density in the results of DPPP structures predicted using (a) Dreiding forcefield and (b) COMPASS forcefield. Each solid symbol depicts the best fitted structure to the X-ray crystal structure.

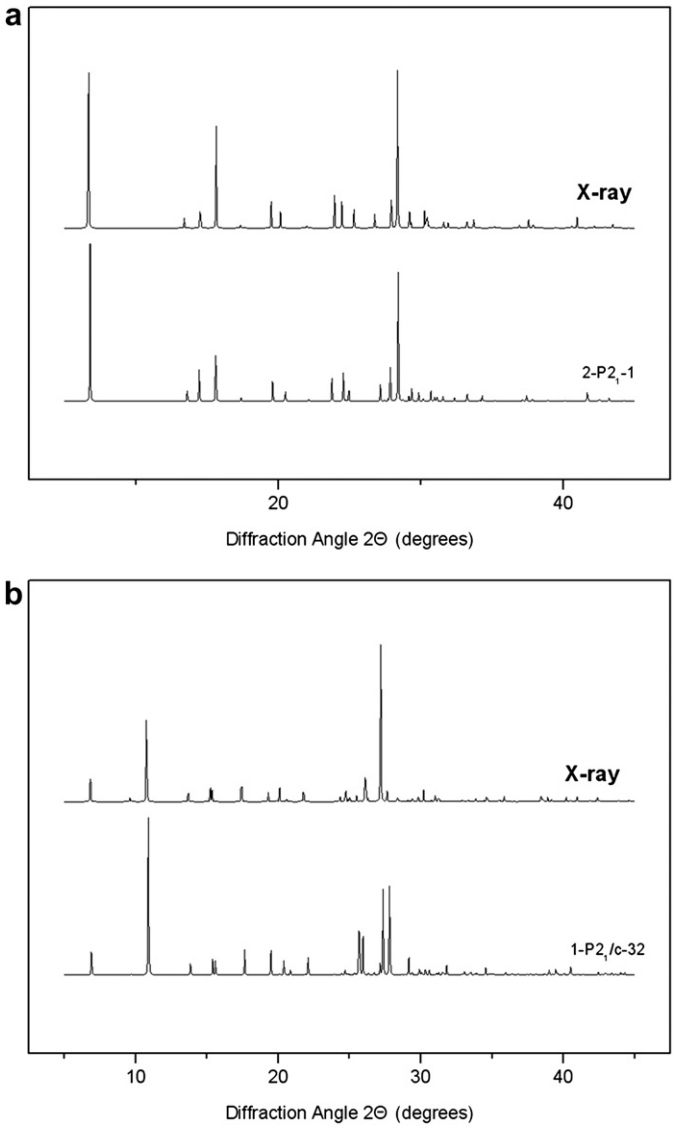


**Fig. 9.** The simulated powder patterns of the X-ray and predicted structures of DPPP which are from the results with COMPASS for (a) phase I and (b) phase II.

Fig. 12 shows the simulated XRPD pattern of the structure predicted using Dreiding forcefield. In contrast to the result of COMPASS, the phase II crystal structure is well predicted with Dreiding forcefield. The XRPD patterns of predicted and X-ray of DPPP phase II is very similar. But, in the case of phase I, the peak intensity and position have small differences and it comes from the difference of unit cell dimensions and the torsional angles of the molecule.

## 4. Summary

We performed crystal structure prediction for DPP and DPPP. These two organic pigments have almost similar molecular structures but different crystal structures. Using the polymorph prediction tools with COMPASS and Dreiding forcefields and the Hartree–Fock level ESP charge, the DPP and DPPP crystal structures could be predicted with high accuracy. In spite of the conformational difference between the input X-ray structures, the prediction process could correctly predict the DPPP phase II structure showing that Monte Carlo simulated annealing is an useful method for predicting the crystal structures of DPP derivatives.

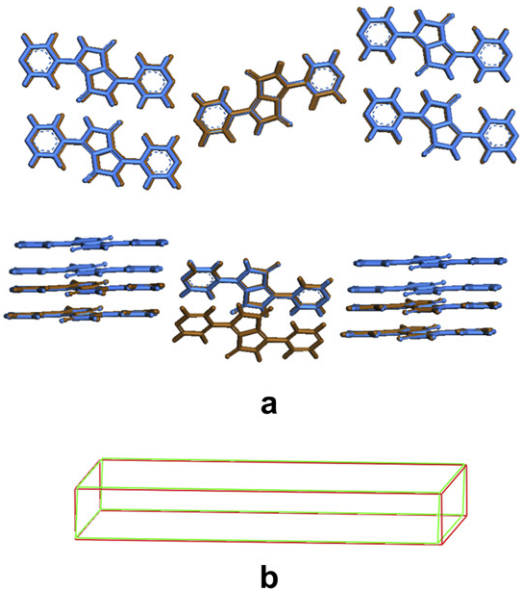


**Fig. 10.** (a) Comparison of the packing shapes of the X-ray structure (blue) and the simulated structure (brown) of DPPP (phase I) which was predicted with COMPASS forcefield. (b) An overlay of the unit cells of the X-ray (red) and predicted (green) structures. (For the interpretation of the reference to color in this figure legend the reader is referred to the web version of this article).

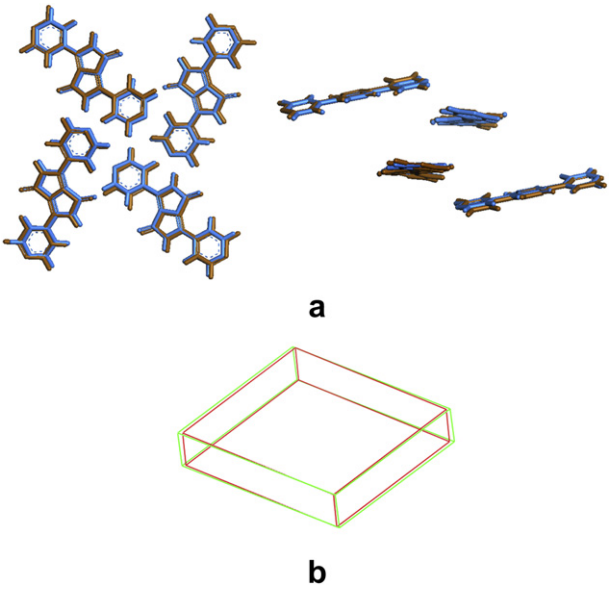


**Fig. 11.** (a) Comparison of the packing shapes of the X-ray structure (blue) and the simulated structure (brown) of DPPP (phase II) which was predicted with Dreiding forcefield. (b) An overlay of the unit cells of the X-ray (red) and predicted (green) structures. (For the interpretation of the reference to color in this figure legend the reader is referred to the web version of this article).

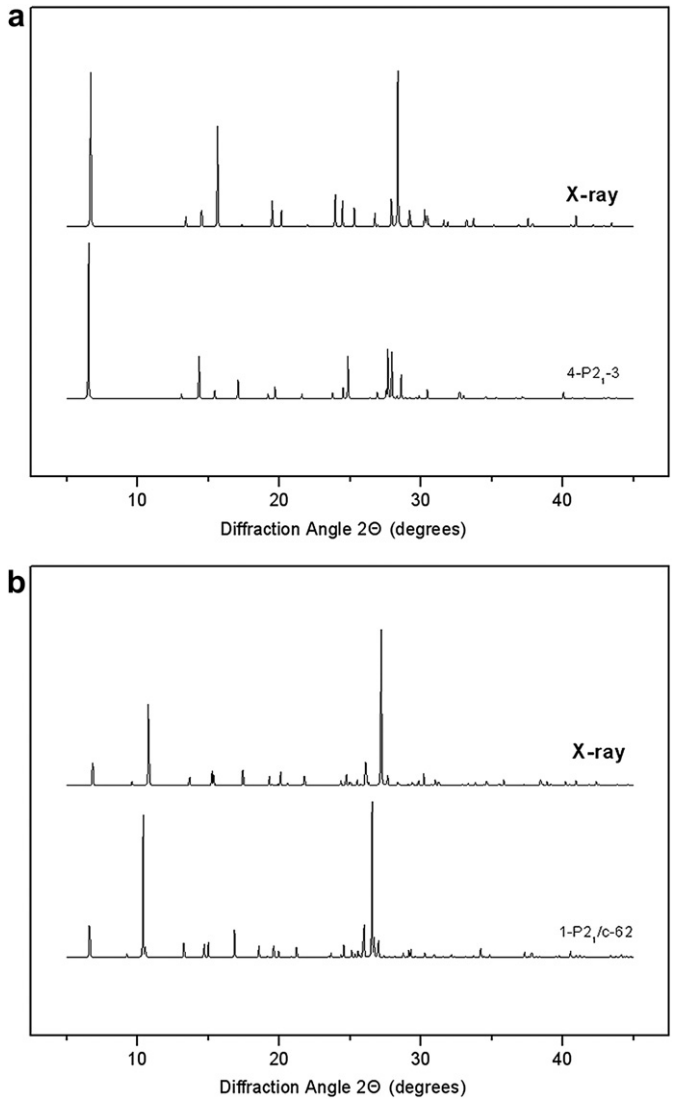


**Fig. 12.** The simulated powder patterns of the X-ray and predicted structures of DPPP which are from the results with Dreiding for (a) phase I and (b) phase II.

## Acknowledgments

This research was performed for the Hydrogen Energy R&D Center, one of the 21st Century Frontier R&D Program, funded by the Ministry of Education, Science and Technology of Korea. We specially thank Accelry Korea for supporting us with the Materials Studio 4.4 software.

## References

[1] Smith H. High performance pigments. Weinheim: Wiley-VCH; 2001.
[2] Park Y-I, Son J-H, Kang J-S, Kim S-K, Lee J-H, Park J-W. Synthesis and electroluminescence properties of novel deep blue emitting 6,12-dihydrodiindeno[1,2-b;1,2-e]pyrazine derivatives. Chemical Communications 2008;18:2143–5.
[3] Klebe G, Graser F, Hadicke E, Berndt J. Crystallochromy as a solid-state effect: correlation of molecular conformation, crystal packing and colour in perylene-3,4:9,10-bis(dicarboximide) pigments. Acta Crystallographica Section B 1989;45:69–77.
[4] Leusen FJJ. Ab initio prediction of polymorphs. Journal of Crystal Growth 1996;166:900–3.
[5] Verwer P, Leusen FJJ. Reviews in computational chemistry. Wiley-VCH; 1998.
[6] Erk P, Hengelsberg H, Haddow MF, van Gelder R. The innovative momentum of crystal engineering. Crystal Engineering Communications 2004;6(78):474–83.
[7] Panina N, vand de Ven R, Verwer P, Meekes H, Vlieg E, Deroover G. Polymorph prediction of organic pigments. Dyes and Pigments 2008;79:183–92.
[8] Price SL. From crystal structure prediction to polymorph prediction: interpreting the crystal energy landscape. Physical Chemistry Chemical Physics 2008;10:1996–2009.
[9] Thun J, Schoeffel M, Breu J. Crystal structure prediction could have helped the experimentalists with polymorphism in benzamide. Molecular Simulation 2008;34:1359–70.
[10] Lommerse JPM, Motherwell WDS, Ammon HL, Duntiz JD, Gavezzotti A, Hofmann DWM, et al. A test of crystal structure prediction of small organic molecules. Acta Crystallographica Section B: Structure Science 2000;56:697–714.
[11] Motherwell WDS, Ammon HL, Duntiz JD, Dzyabchenko A, Erk P, Gavezzotti A. Crystal structure prediction of small organic molecules: a second blind test. Acta Crystallographica Section B: Structure Science 2002;58:647–61.
[12] Day GM, Motherwell WDS, Ammon HL, Boerrigter SXM, Valle RGD, Venuti E. A third blind test of crystal structure prediction. Acta Crystallographica Section B: Structure Science 2005;61:511–27.
[13] Day GM, Cooper TG, Cruz-Cabeza AJ, Hejczyk KE, Ammon HL, Boerrigter SXM, et al. Significant progress in predicting the crystal structures of small organic molecules – a report on the fourth blind test. Acta Crystallographica Section B: Structure Science 2009;65:107–25.
[14] Herbst M, Hunger K. Industrial organic pigments. Weinheim: VCH; 1993.
[15] Mizuguchi J. Solution and solid state properties of 1,4-diketo-3,6-bis-(4-pyridyl)-pyrrolo-[3,4-c]-pyrrole on protonation and deprotonation. Ber Bunsenges Physical Chemistry 1993;97:684–93.
[16] Frisch MJ, Trucks GW, Schlegel HB, Gill PMW, Johnson BG, Robb MA. Gaussian 04 (revision C.02). Pittsburgh, PA: Gaussian Inc; 2004.
[17] Materials studio 4.4. Accelrys; 2009.
[18] Rigby D, Sun H, Eichinger BE. Computer simulations of poly(ethylene oxide): forcefield, PVT diagram and cyclization behavior. Polymer International 1998;44:311–30.
[19] Sun H. COMPASS: An ab initio forcefield optimized for condensed-phase application-overview with details on alkane and benzene compounds. The Journal of Physical Chemistry B 1998;102:7338–64.
[20] Sun H, Ren P, Fried JR. The COMPASS forcefield: parameterization and validation for phosphazenes. Computational and Theoretical Polymer Science 1998;8:229–46.
[21] Mayo SL, Olafson BD, Goddard WAI. DREIDING: a generic force field for molecular simulations. The Journal of Physical Chemistry 1990;94:8897–909.
[22] Rappe AK, Goddard WA. Charge equilibration for molecular dynamics simulations. The Journal of Physical Chemistry B 1991;95:3358–63.
[23] Gasteiger J, Marsili M. Iterative partial equalization of orbital electronegativity – a rapid access to atomic charges. Tetrahedron 1980;36:3219–88.
[24] Mizuguchi J, Imoda T, Takahashi H, Yamakami H. Polymorph of 1,4-diketo-3,6-bis-(4′-dipyridyl)-pyrrolo-[3,4-c]-pyrrole and their hydrogen bond network: a material for $H_2$ gas sensor. Dyes and Pigments 2006;68:47–52.